Torque and Power Capabilities of Coreless Axial Flux Machines with Surface PMs and Halbach Array Rotors

Yaser Chulaee[1], Donovin Lewis[1], Matin Vatani[1], John F. Eastham[2], and Dan M. Ionel[1]
[1]SPARK Laboratory, ECE Department, University of Kentucky, Lexington, KY, USA
[2]University of Bath, Claverton Down, Bath, BA2 7AY, UK
yaser.chulaee@uky.edu, donovin.lewis@uky.edu, matin.vatani@uky.edu, jfeastham@aol.com, and dan.ionel@ieee.org

***Abstract*—This paper investigates employing a Halbach PM rotor array to increase torque and power density within coreless axial flux permanent magnet (AFPM) machines. Analytical and 2/3-dimensional finite element analysis (FEA) methods are developed to study torque and power capabilities within an example double-rotor, single-stator coreless AFPM machine with a PCB stator. Compared to a surface PM topology of the same mass and volume, employing a Halbach array increases torque density by as much as 30% through increased airgap flux density amplitude. Multiple parametric studies are performed to explore methods of increasing torque and power density while employing Halbach arrays combined with enhanced cooling methods and coil transposition to minimize associated losses. A design procedure is also developed that relies on the advantages of coreless AFPM machines controlled by ultra-high-frequency SiC-based drive systems to maximize potential torque gain.**

***Index Terms*—Axial-flux, coreless machines, AFPM machines, permanent-magnet machines, Halbach-array, PCB stator, FEA, eddy current.**

I. Introduction

Axial flux permanent magnet (AFPM) synchronous machines are experiencing a growing demand for a wide range of applications, such as HVAC systems, electric vehicles, aircraft propulsion, etc. due to their high power density and compact structure. The coreless stator type topology eliminates the magnetic cores and the associated core losses, resulting in potential manufacturing simplification, increased efficiency, no cogging torque, and reduced weight and volume, all of which contribute to a higher overall efficiency and torque density. One of the early developments of a coreless axial flux machine with multiple rotors designed for electric aircraft propulsion has been described in [1], [2]. Removal of the stator core results in lower airgap flux density and a lower quality sinusoidal airgap flux density compared to cored AFPM machines [3], [4]. Moreover, without the protection of slots, windings in coreless AFPM machines are directly exposed to airgap flux density variations, causing eddy currents within the stator conductors. Flux fringing and non-uniformly distributed flux density are also common in machines with wide magnetic airgaps and lead to circulating current losses in parallel conductors [5]–[7].

To improve the amplitude of the airgap flux density, one typical solution is to employ a Halbach-array PM arrangement, which is an array of discrete PM segments whose magnetization vectors are at various angles with respect to the axial direction [8]. Halbach array PM rotors eliminate the need for a rotor back iron, resulting in higher torque density due to reduced active material and eliminating eddy current loss in the backing iron due to stator winding space harmonics. Halbach array rotor configuration also forms a more sinusoidal airgap flux density, leading to smoother machine operation.

Increasing popularity of Halbach array integration with coreless machines can be attributed to their ability to generate high specific power. The performance of two coreless axial flux PM machines, one with a Halbach array and the other with a spoke-type PM rotor, were designed and compared for indirect drive in-wheel motors of unmanned ground vehicles in [9]. The results indicate that the motor with a Halbach-array PM rotor exhibits approximately 28% higher output torque, implying a higher torque density and efficiency compared to the spoke-type PM rotor. A high-speed Halbach array coreless AFPM machine is suggested and investigated in [8] to validate the efficacy of a high-speed Halbach array PM rotor by taking into account the mechanical strength, rotor dynamics, and severity of the attractive force between PM segments. The design parameters that affect power density and efficiency of a double sided Halbach array PM ironless AFPM motor were identified and studied in [10]. The set of parameters consists of both geometric and higher-order attributes, which comprise the number of poles, rotor velocity, current density, magnet, winding, and air gap geometries.

Similarly, Halbach array rotors have also been employed in yokeless and segmented armature topologies to achieve high torque densities for electric aircraft applications. A YASA motor with segmented Halbach array magnets and rectangular wires for a 250 kW electric aircraft propulsion application was proposed in [11]. The 3D FEA findings indicate that the motor is capable of achieving the target torque density with an electromagnetic efficiency of 94%. The impact of different slot-pole configurations on the losses and other performance parameters of a dual-rotor Halbach AFPM machine with fractional-slot concentrated winding, using additive manufacturing coils was discussed in [12].

Lack of a magnetic core presents an opportunity to incorporate printed circuit board (PCB) stators in coreless AFPM

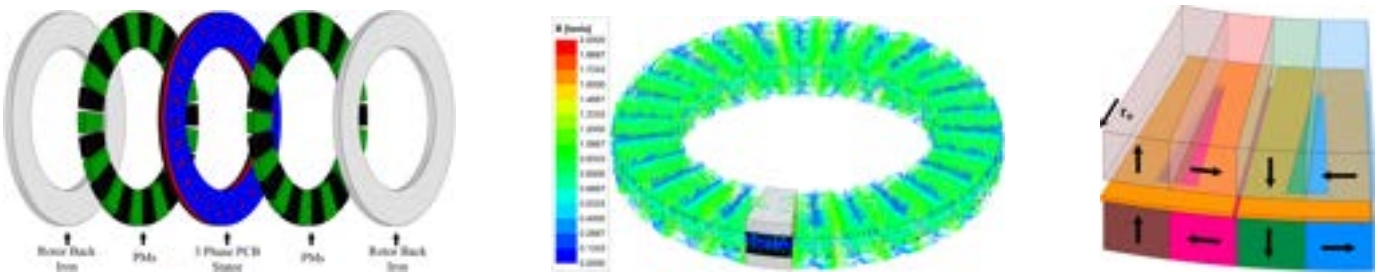

(a) (b) (c)

Fig. 1. An exploded view of the studied 26-pole three-phase double-rotor single-stator coreless AFPM machine with a PCB stator (a), full model flux density lines out of 1/26 of the machine model using symmetry boundaries to reduce computational burden (b), and a 3D FEA segment of the machine for output torque calculation with Halbach array PMs and magnetization direction (c).

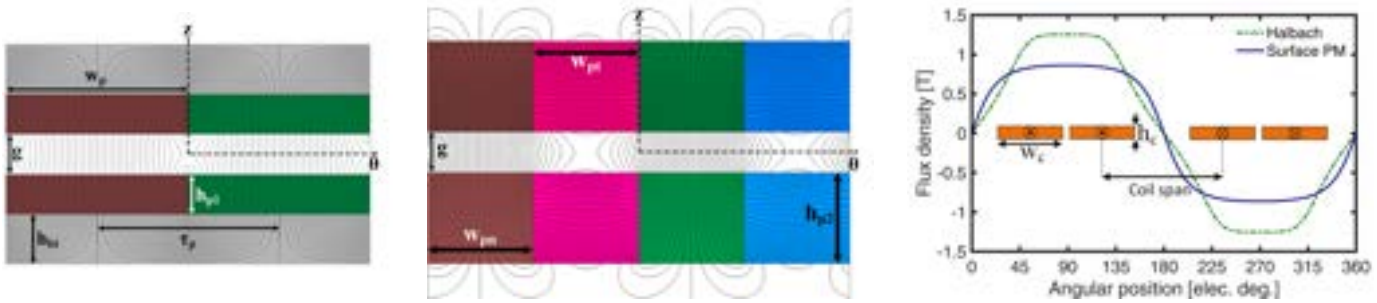

(a) (b) (c)

Fig. 2. The 2D FEA model of the double-sided coreless AFPM machine with conventional surface-mounted PMs (a), coreless AFPM machine with Halbach array rotor (b). Flux density waveforms for the surface PM and Halbach array rotor configurations with rectangles representing stator conductor cross sections (c).

machines, which have gained popularity due to their potential for reliable and highly repeatable fabrication, capability for modularity, and lightweight nature [13], [14]. The high level of flexibility in PCB coil geometry with minimal impact on manufacturing setup enables optimization and design to mitigate stator losses and improve torque production capability [15].

In this paper, the effects of Halbach array PM configuration on the performance of a double rotor, single PCB stator coreless AFPM machine is investigated through comparison with surface PM rotors, relying on analytical equations and finite element analysis (FEA). The results of the analytical equations and FEA models have been verified through the experimental results of a prototype coreless AFPM machine. Potential solutions for further improving the machine's performance by better utilizing Halbach arrays and integrating PCB stators are also discussed.

II. Machine Topologies, Analytical and FEA Modeling

The investigated surface PM coreless AFPM machine uses multiple PCB stators and two external rotors with PMs mounted on rotor back irons, as its exploded view is shown in Fig. 1a. Coreless electric machines are vulnerable to induced stator eddy currents and circulating currents caused by increased exposure to airgap flux density variation without the protection of core slots. The inclusion of PCB stators can greatly mitigate AC losses with precise modeling and design of the planar copper conductor traces, increasing overall efficiency while maintaining compactness [16]. Due to the circumferential and axial periodicity of the machine, 2D and 3D FEA models of one pole or pole pair of the machine have been considered. This simplification considerably reduces the computational time [7]. The full model flux density lines out of 1/26 of the machine model using symmetry boundaries are demonstrated in Fig. 1b. An experimental prototype of the surface-mounted PM configuration has been developed previously and was used to verify models created to approximate overall performance.

To investigate airgap flux densities in detail, 2D FEA models of a cross section of the machine were designed in were designed in Ansys Maxwell [17] with surface-mounted PM and Halbach array rotors. The 2D FEA models within introductory investigations maintain simulation effectiveness while reducing computational time. Example flux lines are shown for the 2D models with the surface PM rotor, Fig. 2a, and the Halbach array rotor, Fig. 2b. Significant neutralization of flux on one side of the magnet boundary enabled the removal of the rotor-back iron within the Halbach rotor variant such that comparable axial length was maintained by increasing the magnet thickness.

The introduction of the Halbach array configuration was

found to increase flux density within the airgap. A 3D FEA model of the Halbach array rotor variant was created with 4 magnets covering 2 stator coils, one pole pair, for accurate torque evaluation and to simulate the expected magnification and cancellation behavior resulting from varied magnetization directions within the Halbach array, as indicated by the arrows in Fig. 1c. The machine, of the same mass and volume as the conventional magnet type, was designed to compare performance, including specific power, torque density, and goodness.

For the double sided surface PM structure shown in Fig. 2a, based on [3], [4], the fundamental component of airgap flux density in the axial direction can be expressed as:

$$\begin{aligned} B_z(\theta, z) &= B_{pk} \cosh\left(\frac{\pi}{\tau_p} z\right) \cos(\theta)\,; \\ B_{pk} &= \frac{4B_r}{\pi} \frac{\sinh(\pi(h_{p1}/\tau_p))}{\sinh(\pi(g/2\tau_p))} \sin\left(\frac{\pi w_p}{2\tau_p}\right), \end{aligned} \tag{1}$$

where B_r is the remanence for the permanent magnets, w_p is the width of PMs and τ_p is the pole pitch, respectively with all being shown on a cross section at a fixed radius, r, in polar coordinates. A similar equation can be derived from Maxwell's equations for the Halbach array rotor variant as follows:

$$\begin{aligned} B_z(\theta, z) &= 2B_{pk} \exp(-\alpha g/2) \cos(\theta) \cosh(\alpha z); \\ B_{pk} &= B_r \left[1 - \exp(-\alpha h_{p2})\right] \frac{\sin(\pi/n_m)}{\pi/n_m}, \end{aligned} \tag{2}$$

where $\alpha = \pi/(w_{pn} + w_{pt})$, h_p is magnet thickness and n_m is the number of magnets within a Halbach array block [4], [5].

The overall thickness of the surface PM rotor, including the back iron ($h_{p1} + h_{bi}$), is equal to the overall thickness of the Halbach rotor. As a result, these two designs are comparable in terms of volume and weight. Similarly, the width of magnets in the Halbach rotors, $w_{pn}+w_{pt}$ is equivalent to the width of a single magnet in the surface-mounted PM rotor, w_p. It should be noted that the selected strong neodymium magnet with a remenance of 1.3 T has a mass density that is comparable to back iron steel. According to (1) and (2), the normal component of airgap flux density, B_z, that contributes to torque production varies in the axial direction proportionally to a hyperbolic sinusoid, with a minimum in the middle of the airgap and an increase towards the PMs in both directions.

Torque is analytically derived from the Lorentz force law as the integral across stator conductor elements in the radial direction when they carry the stator current and are exposed to airgap flux density. The single-phase peak torque is expressed in the following equation:

$$\begin{aligned} \widehat{T}_{ph} &= \int_{r_i}^{r_o} \int_{0}^{\pi} \int_{-h_c/2}^{+h_c/2} N_c \cdot J_s(\theta) \cdot B_z(\theta, z) r \,\mathrm{d}z \,\mathrm{d}\theta \,\mathrm{d}r\,; \\ J_s(\theta) &= \begin{cases} 0 & 0 \le \theta < \frac{\pi(\tau_p - 2w_c)}{2\tau_p} \\ J_m & \frac{\pi(\tau_p - 2w_c)}{2\tau_p} \le \theta < \frac{\pi(\tau_p + 2w_c)}{2\tau_p} \\ 0 & \frac{\pi(\tau_p + 2w_c)}{2\tau_p} \le \theta < \pi \end{cases}, \end{aligned} \tag{3}$$

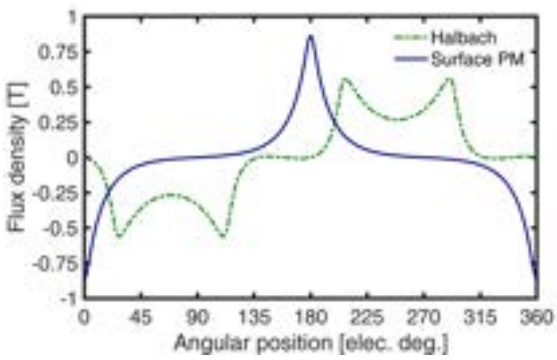

Fig. 3. The tangential component of airgap flux density, B_t, over the stator surface in both designs.

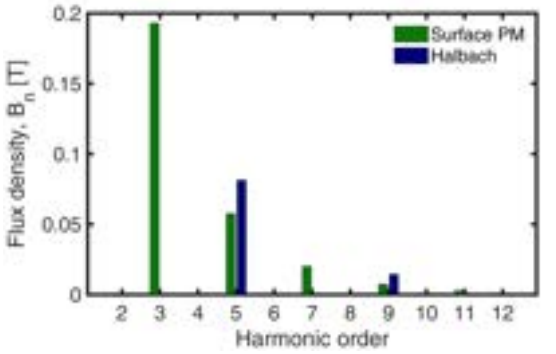

Fig. 4. Harmonic content of the airgap flux density with fundamental omitted for surface PM and Halbach array rotor configurations. The fundamental component of surface PM and Halbach array is 1.01 T and 1.32 T, respectively.

where w_c is coil width, r_o the coil outer radius, r_i the coil inner radius, N_c the number of coils in series per phase, J_m is the maximum current density, and r the distance from the shaft to the conductor element in the radial direction. Equation (3) highlights that modifying stator coil orientation to overlap with the period of maximum flux density can maximize torque output within either machine. The following section discusses FEA and analytical results derived from the analytical equations and introduced FEA models.

III. Numerical and Experimental Performance Evaluation

Numerous observations can be found through the analysis of the airgap flux density waveforms. The normal component of the airgap flux density waveforms in middle of airgap, $z = 0$, for both surface PM and Halbach array configurations relative to angular electrical degree within one pole pair is illustrated in Fig. 2c. The position of stator coils with respect to the airgap flux density to maximize torque is also demonstrated in the aforementioned figure. In this design, the PCB thickness per phase is 1 mm, and the mechanical airgap is 1 mm for each side, such that the total magnetic airgap, magnet to magnet distance, M2M, is 5 mm. The peak value of the airgap flux density is increased by 45% through the use of

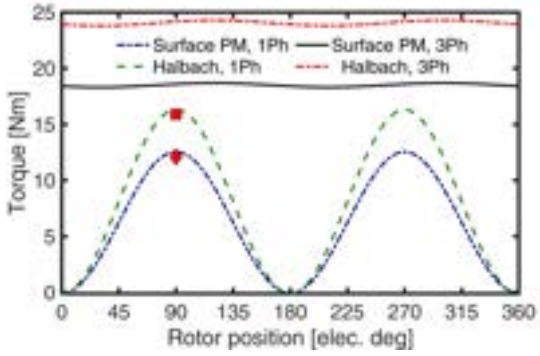

Fig. 5. Torque waveforms for the conventional and Halbach array variant in single and three phase; the analytically calculated maximum values based on (3) are marked on the figure.

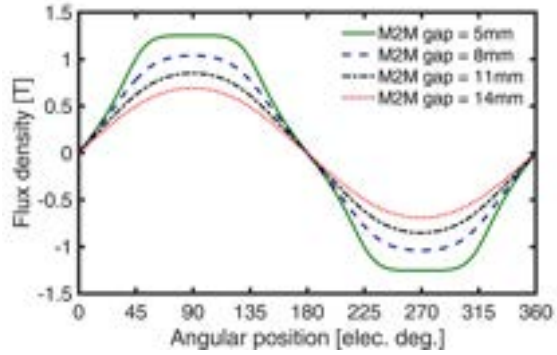

Fig. 6. Airgap flux density at varying magnetic airgaps. For the Halbach array rotor variant, all waveforms are shifted for comparison purposes.

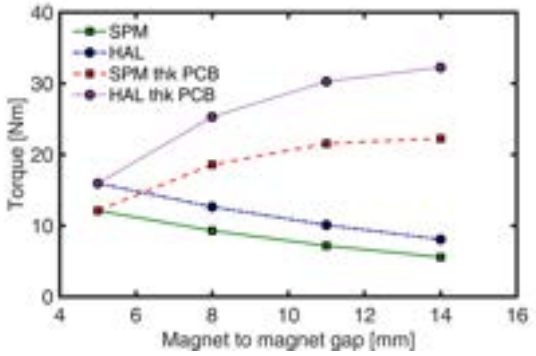

Fig. 7. Output torque at wider magnet-to-magnet gaps for surface PM, SPM, and Halbach array (HAL) rotors with constant and modified ampere-turn. Two curves denoted by "- thk PCB" represent the output torque values when the ampere-turn of thicker PCBs was modified accordingly.

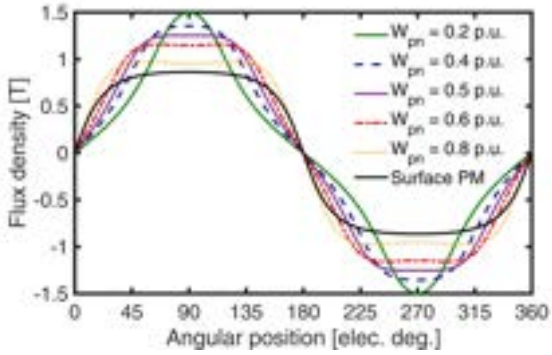

Fig. 8. Airgap flux density with varying normal component permanent magnet widths. For the Halbach array rotor variant, all waveforms are shifted for comparison purposes.

Halbach arrays. Following Fig. 2c, Halbach array flux density has a more sinusoidal waveform than the conventional one. The results of the harmonic analysis demonstrated in Fig. 4 show that the amplitude of the fundamental component improves by 30% with the smaller values for other harmonic orders, resulting in potentially increased torque at the same current density, smoother operation, and lowered eddy current losses. Interaction of the tangential component, B_t, with stator currents applies attraction and repulsion forces on the stator surface, resulting in vibration and noise-related degradation. As shown in Fig. 3, the amplitude of the B_t for the Halbach array is reduced by approximately 50% and is more balanced, which mitigates instantaneous forces on the stator surface.

From 3D FEA, the output torque, depicted in Fig. 5, increased by 30% from the conventional surface-mounted PMs to the Halbach array rotor with the same mass, volume, current density, and temperature rise in single and three-phase variants. Torque density of the machine under study increases by the same amount and reaches 3.45 Nm/kg at the rated speed of 2100 rpm. It should be noted that due to the very low armature reaction and lack of saturation effect in coreless machines, the torque waveform is approximately sinusoidal, and hence the output torque can be derived by calculating the maximum value. The analytically calculated maximum torques for both topologies are marked on the torque waveforms at 90 elec. degrees and show a good agreement between FEA and analytical results.

Further improvement in torque density can be achieved by the optimal use of Halbach array PM rotors in combination with higher current densities or ampere-turns and enhanced cooling systems. For example, doubling the PCB thickness per phase to accommodate double ampere-turns, leading to an M2M gap of 8 mm, decreases the amplitude of the airgap flux density by 20%, as shown in Fig. 6. It can be said that higher ampere-turns can effectively compensate for the effect of lower flux density due to the wider gap. The computational results illustrated in Fig. 7 indicate that at higher electric loads achieved through a larger magnet-to-magnet airgap filled in with thicker PCBs with high equivalent ampere-turns, the Halbach design can deliver approximately 50% more torque within the same total envelope, resulting in a significantly higher power density. The implementation of such designs requires, of course, special cooling solutions for the higher losses in the stators placed in between the rotors.

The effect of normal component magnet width, w_{pn}, on the airgap flux density was also studied with results in Fig. 8 with

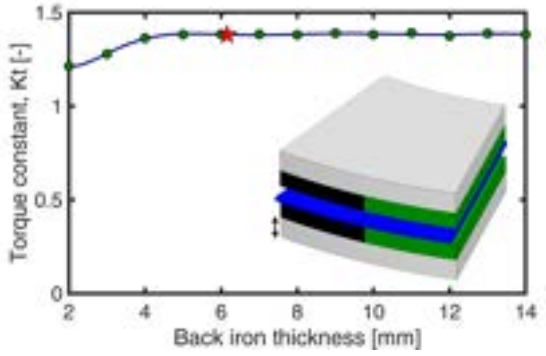

Fig. 9. Results of the parametric study to determine the minimum thickness of rotor back iron to avoid saturation. The thickness of rotor back iron for the machine under study is denoted by ⋆.

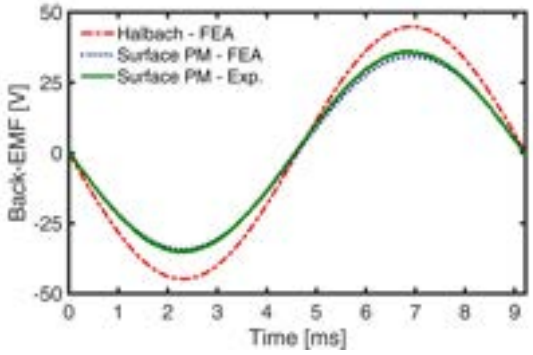

Fig. 10. Measured and calculated back-EMF waveforms for surface PM and Halbach array configurations.

the per unit base of the pole pitch, $\tau_p = w_{pn} + w_{pt}$. Varying the ratio of normal magnet width to tangential in the Halbach array topology modifies the resulting airgap flux density in terms of amplitude and coil coverage, allowing for optimization of torque according to this ratio. It can be inferred that utilizing normal and tangential magnets with identical widths represents the optimal choice with regard to both amplitude and coil coverage of the airgap flux density.

A parametric study was carried out to determine the thickness of rotor back iron to avoid saturation as shown in Fig. 9. The torque constant across a wide range of rotor thickness may be used to calculate the minimum thickness of rotor back iron. When it reaches a constant value, the matching thickness can be employed. To verify the accuracy of the designed 3D FEA models, the measured back-EMF of the prototype machine is compared with the FEA results for both surface PM and Halbach array rotors as illustrated in Fig. 10. The experimental prototype machine along with the machine components, a permanent magnet rotor, and a PCB stator are shown in Fig. 11.

IV. Comparative Studies and Discussions

Airgap flux density in coreless machines is not evenly distributed both in normal and tangential directions, as can be seen in the flux density lines in Fig. 2b. Widening the

Fig. 11. The experimental prototype machine employed for model verification.

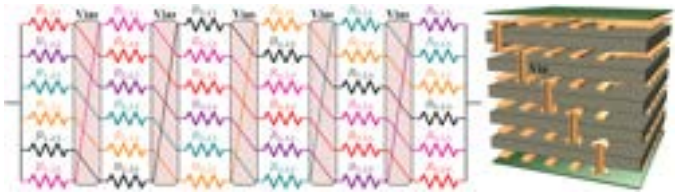

Fig. 12. Example stator coil interconnections with layer transposition in a PCB stator to balance induced voltages and mitigate circulating currents.

magnetic airgap to increase ampere-turn will magnify the uneven airgap flux distribution, leading to different induced voltages in stator conductors. Voltage differences in parallel conductors cause circulating currents that can be mitigated through PCB conductor transposition between layers, with an example strategy shown in Fig. 12. Transposition of coil connections balances back-EMF of coil sections, ensuring equal impact by variation in airgap flux density [16].

A systematic approach for initial sizing of coreless AFPM machines can be developed as a basis for future design optimizations. The outer diameter of the machine should be sized based on the intended application, followed by the rated speed defined by mechanical operation constraints and the admissible fraction of the speed of sound for the periferic speed. In cored machines, design limiting factors include the frequency of operation and the number of pole pairs due to their impact on core losses. In axial flux coreless machines controlled by ultra-high frequency drive systems based on wide bandgap devices, the number of pole pairs is no longer a limiting factor, allowing main parameters such as magnet to magnet airgap size relative to pole pitch and pole count to be the focus of design for Halbach array rotors.

When considering the maximization of torque density, the analytical relationship between airgap flux density and geometrical parameters can be used to guide critical design parameters. Airgap flux density has a downward trend when the ratio of magnetic airgap to pole pitch increases, as illustrated by the dotted-dashed line in Fig. 13 rely on equation (2). Due to this trend, increasing the gap between two magnets should accompany an increase in pole pitch to maintain a target ratio and a lower number of pole pairs with a constantly defined

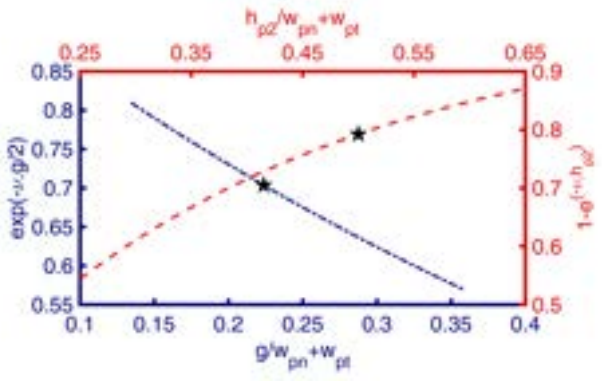

Fig. 13. Flux density changes with respect to Halbach PM magnet geometry including magnet aspect ratio and the airgap to pole pitch. Corresponding ratios to the design under study are marked with stars.

outer diameter. An upward trend exists with the ratio of magnet thickness to pole pitch and the flux density, depicted by the dashed line in Fig. 13. A thicker magnet improves flux density, but it has the adverse impact of reducing torque density due to its increased mass. From this relationship, a lower pole pitch with the same outer diameter results in a higher number of pole count, is a good means of improving torque and power density. To achieve the target torque and power densities, proper selection of pole pairs, pole pitch, magnet thickness, and the number of magnets per pole pair, n_m, is required.

V. Conclusion

This paper investigated the effect of employing Halbach array magnet configurations for rotors in coreless AFPM machines to increase flux density, torque density, and specific power. A systematic comparison was performed between 2D and 3D FEA models for coreless AFPM machines with surface-mounted PMs and one with Halbach array magnets in terms of important performance indices, including torque density and power density, and secondary effects like normal forces on the stator windings. Different parametric studies have been carried out to investigate potential measures to improve torque density within Halbach array PM rotor configurations, combining special techniques for loss mitigation in PCB stators and enhanced cooling systems. The computational results showed that the Halbach design can deliver about 50% more torque within the same total envelope at higher electric loads achieved through a larger magnet-to-magnet airgap filled in with thicker PCBs with high equivalent ampere-turns, leading to a considerably higher power density.

Acknowledgment

This paper is based upon work supported by the National Science Foundation (NSF) under Award No. #1809876. Any opinions, findings, and conclusions or recommendations expressed in this material are those of the authors and do not necessarily reflect the views of the NSF. The support of ANSYS Inc., and University of Kentucky, the L. Stanley Pigman Chair in Power Endowment is also gratefully acknowledged.

References

[1] R. Hill-Cottingham, P. Coles, J. Eastham, F. Profumo, A. Tenconi, and G. Gianolio, "Multi-disc axial flux stratospheric aircraft propeller drive," in *Conference Record of the 2001 IEEE Industry Applications Conference. 36th IAS Annual Meeting (Cat. No.01CH37248)*, vol. 3, pp. 1634–1639, 2001.

[2] F. Profumo, A. Tenconi, M. Cerchio, J. Eastham, and P. Coles, "Axial flux plastic multi-disc brushless pm motors: performance assessment," in *Nineteenth Annual IEEE Applied Power Electronics Conference and Exposition, 2004. APEC '04.*, vol. 2, pp. 1117–1123, 2004.

[3] A. Mohammadpour, A. Gandhi, and L. Parsa, "Winding factor calculation for analysis of back emf waveform in air-core permanent magnet linear synchronous motors," *Electric Power Applications, IET*, vol. 6, pp. 253–259, 05 2012.

[4] N. Chayopitak and D. G. Taylor, "Performance assessment of air-core linear permanent-magnet synchronous motors," *IEEE Transactions on Magnetics*, vol. 44, no. 10, pp. 2310–2316, 2008.

[5] J. Gieras, R.-J. Wang, and M. Kamper, *"Axial Flux Permanent Magnet Brushless Machines"*. 2nd Edition, Springer, Berlin, 2008.

[6] V. Rallabandi, N. Taran, D. M. Ionel, and J. F. Eastham, "Coreless multidisc axial flux pm machine with carbon nanotube windings," *IEEE Transactions on Magnetics*, vol. 53, no. 6, pp. 1–4, 2017.

[7] M. Rosu, P. Zhou, D. Lin, D. Ionel, M. Popescu, F. Blaabjerg, V. Rallabandi, and D. Staton, *"Multiphysics Simulation by Design for Electrical Machines, Power Electronics and Drives"*, J. Wiley - IEEE Press, 2017.

[8] Z. Zhang, C. Wang, and W. Geng, "Design and optimization of halbach-array pm rotor for high-speed axial-flux permanent magnet machine with ironless stator," *IEEE Transactions on Industrial Electronics*, vol. 67, no. 9, pp. 7269–7279, 2020.

[9] C. Wang, J. Han, Z. Zhang, Y. Hua, and H. Gao, "Design and optimization analysis of coreless stator axial-flux permanent magnet in-wheel motor for unmanned ground vehicle," *IEEE Transactions on Transportation Electrification*, vol. 8, no. 1, pp. 1053–1062, 2022.

[10] K. Duffy, "Optimizing power density and efficiency of a double-halbach permanent-magnet ironless axial flux motor," in *2016 52nd AIAA/SAE/ASEE Joint Propulsion Conference*, 2016.

[11] D. Talebi, M. C. Gardner, S. V. Sankarraman, A. Daniar, and H. A. Toliyat, "Electromagnetic design characterization of a dual rotor axial flux motor for electric aircraft," *IEEE Transactions on Industry Applications*, vol. 58, no. 6, pp. 7088–7098, 2022.

[12] P. Kumar and A. M. EL-Refaie, "Effect of slot-pole combination on performance of a dual rotor halbach-array axial flux permanent magnet machine enabled by additively manufactured winding," in *2022 International Conference on Electrical Machines (ICEM)*, 2022, pp. 1962–1968.

[13] D. Lawhorn, P. Han, D. Lewis, Y. Chulaee, and D. M. Ionel, "On the design of coreless permanent magnet machines for electric aircraft propulsion," in *2021 IEEE Transportation Electrification Conference & Expo (ITEC)*, 2021, pp. 278–283.

[14] P. Han, D. Lawhorn, Y. Chulaee, D. Lewis, G. Heins, and D. M. Ionel, "Design optimization and experimental study of coreless axial-flux pm machines with wave winding pcb stators," in *2021 IEEE Energy Conversion Congress and Exposition (ECCE)*, 2021, pp. 4347–4352.

[15] A. Hembel and B. Sarlioglu, "Pcb winding for electric machines with integrated 3d printed heat exchanger," in *2022 IEEE Transportation Electrification Conference & Expo (ITEC)*, 2022, pp. 421–426.

[16] Y. Chulaee, D. Lewis, G. Heins, D. Patterson, and D. M. Ionel, "Winding losses in coreless axial flux pm machines with wave and spiral pcb stator topologies," in *2022 IEEE Energy Conversion Congress and Exposition (ECCE)*, 2022, pp. 1–6.

[17] *Ansys® Electronics, version 21.2, 2021, ANSYS Inc.*